Precision Measurement of $\sin^2\theta_W$ at a Reactor

J. M. Conrad, J. M. Link, M. H. Shaevitz

This paper presents a strategy for measuring $\sin^2\theta_W$ to $\sim 1\%$ at a reactor-based experiment, using $\bar{\nu}e$ elastic scattering. This error is comparable to the NuTeV, SLAC E158, and APV results on $\sin^2\theta_W$, but with substantially different contributions to the systematics. An improved method for identifying $\bar{\nu}p$ events, which serve both as a background and as a normalization sample, is described. The measurement can be performed using the near detector of the presently proposed reactor-based oscillation experiments. We conclude that an absolute error of $\sim \delta(\sin^2\theta_W) = 0.0019$ may be achieved.

This paper outlines a method for measuring $\sin^2\theta_W(Q^2 \approx 0)$ at a reactor-based experiment. The study is motivated by the NuTeV anomaly, a 3σ deviation of $\sin^2\theta_W$ from the Standard Model prediction [1], measured in deep inelastic neutrino scattering ($Q^2 = 1$ to 140 GeV^2, $\langle Q^2_\nu \rangle = 26$ GeV^2, $\langle Q^2_{\bar{\nu}} \rangle = 15$ GeV^2). Various Beyond-the-Standard Model explanations have been put forward, and those which best explain the result require a follow-up experiment which probes the neutral weak couplings specifically with neutrinos, such as the one described here.

This proposed measurement is also interesting as an additional precision study at $Q^2 = 4 \times 10^{-6}$ GeV^2. The two existing low Q^2 measurements are from atomic parity violation[2], which samples $Q^2 \sim 0$; and SLAC E158, a Møller scattering experiment at average $Q^2 = 0.026$ GeV^2 [3]. Using the measurements at the Z-pole with $Q^2 = M_z^2$ to fix the value of $\sin^2\theta_W$, and evolving to low Q^2, Fig. 1 shows that these results are in agreement with the Standard Model. However, the radiative corrections to neutrino interactions allow sensitivity to high mass particles which are complementary to the APV and Møller scattering corrections. Thus, this proposed measurement will provide valuable additional information.

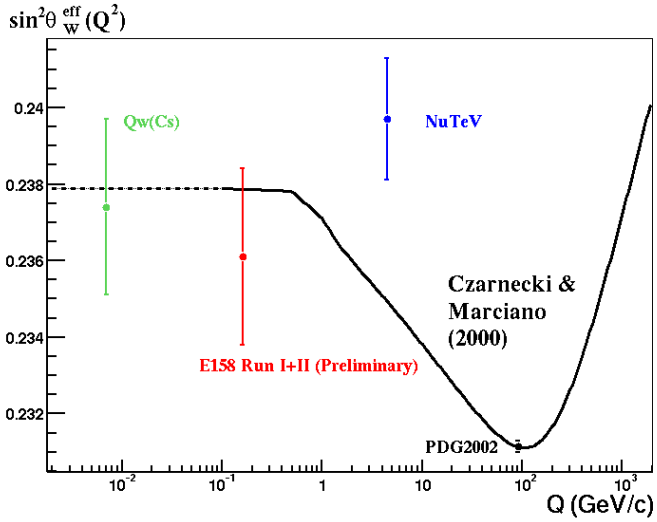

Figure 1: Measurements of $\sin^2\theta_W$ as a function of Q; from reference [4]. The curve shows the Standard Model expectation.

The technique we employ uses the rate of the purely leptonic $\bar{\nu}e$ scattering to measure $\sin^2\theta_W$. This signal was first detected by Reines, Gurr, and Sobel[5], who found $\sin^2\theta_W = 0.29 \pm 0.05$. In this paper, we explore what is necessary to improve on their idea and make a competitive measurement today. One important step is to normalize the $\bar{\nu}e$ "elastic scatters" using the $\bar{\nu}p$ "inverse beta decay" (IBD) events, to reduce the error on the flux. Other crucial improvements are that the detector is located beneath an overburden of ∼300 mwe (meters, water-equivalent) and built in a clean environment. We find that a measurement of ±0.0019 is achievable. This is comparable to the NuTeV error of ±0.0017.

The proposed design employs spherical scintillator oil detectors similar to those used by CHOOZ[6] and by other experiments proposed to measure the oscillation parameter θ_{13}[7]. The detector consists of a spherical central region of Gd-doped scintillator. The radius of the central region is 190 cm; for this analysis, however, the fiducial volume will be confined to 150 cm. This is surrounded by an undoped scintillator region which extends to a radius of 220 cm. This, in turn, is surrounded by a pure oil region out to a radius of 290 cm, which acts as a buffer between the active detector and the

phototubes.

This style of detector has been optimized to reconstruct $\bar{\nu}p$ events, which dominate the rate when the reactor is running. We show, however, that this design is also optimal for measuring $\sin^2\theta_W$ to high precision. Initially, one might think otherwise, since the $\bar{\nu}p$ events represent a potential background. We will show, though, that this background can be controlled. In fact, these events are invaluable because they constrain the normalization. This normalization measurement must be done in the same detector as the $\bar{\nu}e$ measurement to exploit cancellations of systematics, especially those related to the fiducial volume.

In order to control backgrounds, this analysis exploits a visible energy "window" from 3 to 5 MeV. We will show that we can obtain significant signal statistics even within this limited region. On the other hand, this range is above most environmental backgrounds in the detector, and below the energy produced by neutron capture in Gd.

This paper is organized in the following manner. First, we identify the important questions which drive the design choices. Second, we provide details of the generic experiment and analysis used for estimates. Third, we discuss $\bar{\nu}e$ event identification and rates. Fourth, we discuss rejection of $\bar{\nu}p$ events. Fifth, we consider backgrounds produced by natural radioactivity and cosmic rays. Sixth, we consider the errors on the $\bar{\nu}p$ normalization sample. Lastly, we discuss how we find the error on $\sin^2\theta_W$.

Our goal is to establish that this analysis is worth pursuing at a reactor-based experiment. Thus the analysis is presented in sufficient detail to address the major questions. Many detailed studies remain to be done, however, as we discuss in the conclusions. In order to present convincing arguments, we have relied on ideas to reduce background which are well-established for our "standard" calculation of the error on $\sin^2\theta_W$. We also note more speculative ideas which appear promising for further improvement.

1 Introduction to the Design Issues

NuTeV has made a 0.75% measurement, including statistics and systematics, of the weak mixing angle. To match this at the reactor experiment, one needs to measure the $\bar{\nu}e$ absolute rate within the 3 to 5 MeV visible energy window with a 1.2% uncertainty. With this in mind, in order to establish the design for this experiment, the following questions must be explored:

1. Are there sufficient elastic scattering events to perform this measurement?

2. Can the environmental backgrounds be controlled?

3. Can the elastic scattering events be isolated from the inverse beta decay events?

4. How well can the anti-neutrino flux be known?

This section provides qualitative answers to establish that an error on $\sin^2\theta_W$ comparable to NuTeV is feasible.

This section also provides simple motivations for the major cuts. Briefly sketched, these are: a fiducial volume cut which is well within the Gd-doped region; vetoes for cosmics; an energy window from 3 to 5 MeV; and a timing window to search for neutrons which follow a neutrino interaction. Here, we aim only to address the basic needs and challenges. The specifics on the cuts are described in section 2.3. The consequences of the cuts are explored in sections 3 through 6.

Throughout the paper, we will identify certain backgrounds as "negligible." We define negligible as a contribution to the total error of $\leq 0.1\%$. In the case of backgrounds to the signal, this will be < 10 events.

1.1 Statistics

The signal sample consists of elastic scattering events. We call these the "Elastic Sample." A $\leq 1\%$ statistical error, corresponding to $\geq$10,000 elastic events, is necessary if the goal is a total error of $\sim 1.2\%$.

When calculating the total expected events, it must be kept in mind that a visible energy window from 3 to 5 MeV will be necessary to reduce backgrounds. This can be introduced without compromising the required statistics for the signal. Unlike a neutrino magnetic moment analysis[8], which is often the goal for elastic scattering studies at reactors, the measurement of $\sin^2\theta_W$ does not rely on low visible energy events. In fact, we will show in section 3 that the sensitivity is enhanced with a cut on minimum visible energy.

The number of elastic scattering events and inverse beta decay events scale together. Since our premise is to use near detectors for the θ_{13} measurement, which utilizes inverse beta decay events, it is instructive to understand

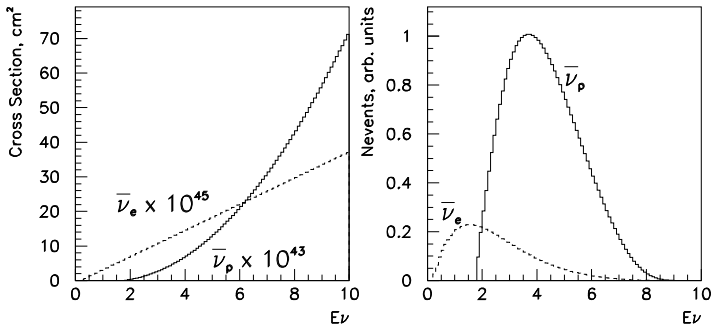

Figure 2: Left: Comparison of $\bar{\nu}e$ and $\bar{\nu}p$ cross sections as a function of neutrino energy in MeV. Right: Comparison of event rates for $\bar{\nu}e$ and $\bar{\nu}p$ as a function of neutrino energy in MeV. Note that electron targets exceed free proton targets in the oil by a factor of 4.3.

the relative rates of these two processes. Fig. 2 (left) compares the cross sections for these interactions as a function of neutrino energy in MeV, scaled for convenience. Fig. 2 (right) compares the unscaled number of events of each type which will be produced. At low energies, where $\bar{\nu}p$ is kinematically suppressed, elastic scattering dominates. Finally, Fig. 3 compares the absolute event rates as a function of visible energy in the detector. The elastic scattering events peak at low visible energy due to the energy carried away by the outgoing neutrino. From Fig. 3, one can see that if greater than 1×10^6 $\bar{\nu}p$ events can be collected within the visible energy window, then the necessary statistical precision on elastic scattering can be reached.

Based on this, we require a design which results in $> 1 \times 10^6$ $\bar{\nu}p$ events. This goal is in concert with the requirements for a near detector for a θ_{13} measurement [7]. The designs under consideration build on the past experience of the CHOOZ experiment, which observed ∼3000 inverse beta decay events in a 5 ton detector located 1 km from two 4.5 GW reactors, running for 132 days effective full power [6]. The proposed near detectors are typically located about 200 m from the reactor, gaining a factor of 25 from solid angle. The detector will be built with increased fiducial mass. Multiple detectors can be built. The experiment can feasibly run longer. In summary, the nec-

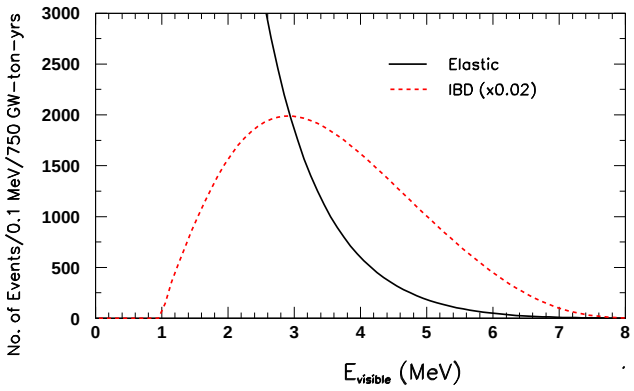

Figure 3: Visible energy distribution for inverse beta decay (red, dashed) and elastic scattering events (black, solid). Inverse beta decay events are scaled by the factor 0.02 to allow visual comparison.

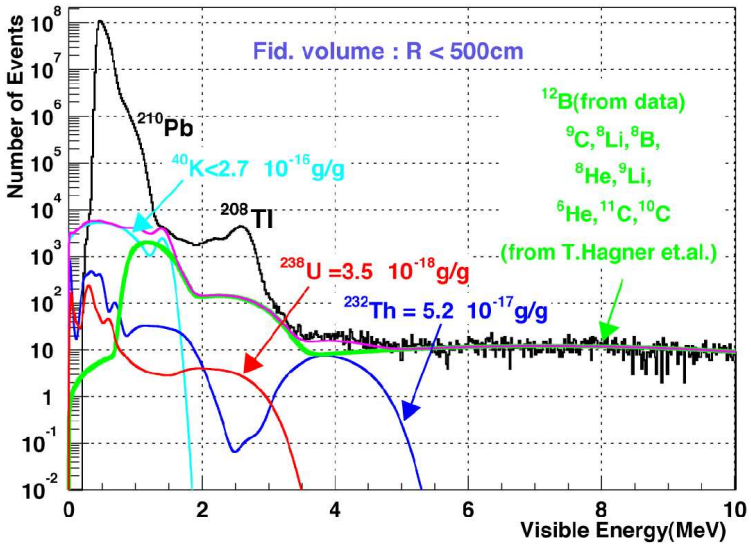

Figure 4: Energy distribution and sources of singles events in KamLAND as a function of visible energy, from reference [9].

essary event rate appears to be attainable with reasonable modifications to the CHOOZ setup.

1.2 $\bar{\nu}p$ Mis-identification

Inverse beta-decay events are a major component of the reactor-on rate in the proposed visible energy window. The best method for separating these events from elastic scatters is observation of the signal from neutron capture. This will motivate a fiducial volume cut which is well within the Gd-doped region in order to assure high efficiency for capturing the neutron. It will also motivate a DAQ system which is sensitive to neutron capture on H, which occurs 16% of the time despite the Gd doping. Lastly, it will motivate an efficient time-window for the neutron search. These are all discussed in detail in section 4.

1.3 Environmental Backgrounds

Environmental backgrounds are by far the most important issue in the analysis and therefore deserve substantial introduction here. These fall into two categories: naturally occurring radioactivity and muon-induced backgrounds. To get a sense for what is expected, Fig. 4 shows the visible energy distribution of singles events from KamLAND with the sources of environmental background identified. The naturally occurring radioactive contaminants mainly populate the low energy range of Fig. 4 and can be kept under control by maintaining KamLAND standards of oil cleanliness. Note that, unlike KamLAND, this experiment will use Gd-doped scintillator, and so the Gd also must be purified of radioactive contaminants also. The other source of environmental background, the β-decays of muon-induced isotopes, populate the higher energy range of Fig. 4.

To reduce background from radioactivity, we introduce spatial and energy cuts. Activity from the tank walls, the phototubes, and the acrylic vessel separating the Gd-doped and undoped regions can be removed by a strong fiducial volume cut. Note that Fig. 4 shows the KamLAND singles rate with a cut of 1.5 m from the acrylic vessel. Most background from radioactivity dissolved in the scintillator can be removed from the sample through a $3 < E_{vis} < 5$ MeV cut on visible energy, as seen in Fig. 4. However, the ^{232}Th chain produces ^{208}Tl, which decays via a β within our visible energy window. This must be addressed.

Potential background from cosmic rays comes from 1) the muons themselves; 2) electrons from muon decays ("Michel electrons"); 3) ^{12}B decays from μ^- capture; 4) spallation neutrons; and 5) isotopes generated by the high energy muons. The first four are straightforward to reduce. The fifth is, potentially, the most significant background in this analysis.

First, consider the four which are straightforward. Muons which enter the tank can be easily identified by means of the high energy which they deposit. Muons which stop may decay to produce electrons, or capture to produce ^{12}B, which β-decays. The need to identify stopping muons motivates a veto based on a combination of tank hits and lack of hits in a hodoscope below the tank. Neutrons which are produced in combination with a cosmic ray event will be identifiable by their capture. Spallation neutrons which are unassociated with a cosmic ray have two sources. They may be produced outside of the tank and then enter; or they may be produced by high energy muon interactions with the ^{12}C within the tank, but not be associated with

Isotope	Source
^{9}Li	$^{12}\mathrm{C} + \mu \rightarrow 3\mathrm{p} + ^{9}\mathrm{Li} + \mu$
^{8}He	$^{1}2\mathrm{C} + \mu^{-} \rightarrow \mathrm{d} + 2\mathrm{p} + ^{8}\mathrm{He}$; $^{12}\mathrm{C} + \mu \rightarrow 4\mathrm{p} + ^{8}\mathrm{He} + \mu$
^{8}Li	$^{12}\mathrm{C} + \mu \rightarrow 3\mathrm{p} + 1\mathrm{n} + ^{8}\mathrm{Li} + \mu$
^{6}He	$^{12}\mathrm{C} + \mu \rightarrow \alpha + 2\mathrm{p} + ^{6}\mathrm{He} + \mu$
^{9}C	$^{12}\mathrm{C} + \mu \rightarrow 3\mathrm{n} + ^{9}\mathrm{C} + \mu$
^{8}B	$^{12}\mathrm{C} + \mu \rightarrow 3\mathrm{n} + 1\mathrm{p} + ^{8}\mathrm{B} + \mu$

Table 1: Examples of sources of isotopes which β decay producing potential background to this analysis.

the parent cosmic due to a late capture time. The Gd-doped buffer region surrounding the fiducial region provides further protection from incoming neutrons. We will show that the proposed visible energy window eliminates unassociated neutrons within the tank.

Production mechanisms for the fifth source, β-decaying isotopes produced by high energy muons, are listed in Table 1. In Fig. 4, one can see the contribution from these isotopes to the KamLAND singles rate above 3 MeV. These are ^{9}Li, ^{8}He, ^{8}Li , ^{9}C , ^{8}B, all of which have endpoints above 10 MeV; and ^{6}He, which has an endpoint at 3.5 MeV. ^{11}Be, may be produced by $^{12}\mathrm{C} + n \rightarrow ^{11}\mathrm{Be} + 2p$, where the n is produced by a muon interaction. This process is not considered within the "standard analysis" because only an upper limit has been reported [10]. However, we do consider the case where this contribution is equal to the limit under alternative scenarios in section 7. The prediction based on measurements by NA54 [10] is in agreement with the KamLAND singles rate above 3 MeV, as indicated by the smooth line on Fig. 4. This gives some confidence that these sources can be understood.

The most important and straightforward way to reduce the rates of these isotopes is to have a very large overburden. This explains our need for at least 300 mwe of depth. However, it will be necessary to reduce the rate further, and this motivates a scheme to search for the cosmic-ray parent. Because of the long lifetimes of the isotopes, a veto on through-going cosmics will produce intolerable deadtime. However, a veto which identifies the subset of parent cosmics that are accompanied by at least one neutron results in a tolerable rate. This is called a muon-neutron veto, and is described in section 5.5. This veto is the only proposed cut which is not based on past experience.

Days of running:	900 Days
Number of reactor cores:	2
Power of each core:	3.6 GW
Overburden:	300 mwe
Distance to near detectors:	224 m
Number of near detectors:	2
Number of far detectors:	4

Table 2: Overview of general assumptions

1.4 Normalization

Absolute knowledge of the reactor neutrino flux is limited by the $\sim 2\%$ uncertainty on the reactor properties. To avoid this error, we use $\bar{\nu}p$ events (the "Normalization Sample") to establish the normalization for the $\bar{\nu}e$ events. The statistical error on the $\bar{\nu}p$ events is small since there are $> 1 \times 10^6$ events expected. The cross section for $\bar{\nu}p$ is well known from theory, as discussed in section 4, so the systematic error from this source is negligible. An important systematic error comes from determination of the ratio of targets for $\bar{\nu}e$ versus $\bar{\nu}p$ scatters, *i.e.* the electron-to-free-proton ratio. Another important systematic question is related to the n-identification. One can obtain a very pure sample of $\bar{\nu}p$ events by requiring a Gd capture. This, however, will introduce a systematic error from the ratio of Gd captures to the total, which was 1% in CHOOZ. This is unacceptably high for this analysis and must be reduced through improved calibration studies. Alternatively, assuming we can trigger with high efficiency on events with H captures, one can accept all n-identified events into the $\bar{\nu}p$ sample. This eliminates the error on the Gd capture ratio but introduces possible backgrounds from accidental coincidences. Estimating these backgrounds will require a detailed study, beyond the scope of the present work. Therefore, for this analysis, we will use the former method of identifying a clean sample through the Gd captures.

Basic Detector Design Parameters	
Radius of fiducial region	150 cm
Fiducial volume per detector	13 tons
Outer radius of central region	190 cm
Tonnage of the central region	26.5 tons
Outer radius of photon catcher	220 cm
Outer radius of detector	290 cm
Pathlengths of Particles (for Calculation of Containment)	
e^- and e^+ track length	negligible
e^+ to n separation length	6 cm
0.5 MeV γ Compton path length	11 cm
Neutron Parameters (for Calculation of ID Efficiency)	
Fraction of n which capture on Gd (H)	84% (16%)
Neutron capture time	30.5 μs

Table 3: Assumptions related to the detector design used in this paper.

2 The General Design and "Standard" Analysis Cuts

In order to calculate an expected error on $\sin^2\theta_W$, we must make assumptions about the design. A summary of the assumptions is presented in Table 2. We use a setup which is drawn from the Braidwood design for the θ_{13} experiment. We assume two 3.6 GW reactors. The neutrino flux is taken from reference [11]. We assume two near detectors and four far detectors. The near detector hall is 224 m from the two reactors and beneath 300 mwe of overburden. The far detectors are located at 1.8 km from the reactor core. These are used in this analysis to study backgrounds. Spherical detectors with active and passive shielding are envisioned. Data taking is assumed to be 900 live-days.

It is necessary to make some specific assumptions in order to proceed with our calculations. These choices are reasonable and so serve for the proof-of-principle calculation. Small variations of this "generic" plan are expected and can easily be accommodated. Table 3 summarizes the assumptions. We address 1) basic definition of detector regions, 2) assumptions about track length which are relevant to calculating backgrounds, and 3) parameters

related to identification efficiency which are relevant for calculating both backgrounds and the normalization rate.

2.1 The Basic Detector Design

The outer radius of the detector design is chosen to allow the detectors to fit within a 3 m radius tunnel, which can be excavated with standard machinery. The interior sizes are scaled to match this requirement. The detector has a "central region" of Gd-doped scintillator, a "photon catcher" region which surrounds this, and an "oil buffer" region which separates the active regions from the phototubes and tank walls. For the sake of this discussion, we take the outer radius of the central region to be 190 cm. The fiducial region must be of substantially smaller radius to maximize containment of the neutrons produced by $\bar{\nu}p$ events and minimize environmental backgrounds. We will assume a fiducial radius of 150 cm. The Gd-doped region is surrounded by a 30 cm "photon catcher" of scintillator with no Gd doping. The photon catcher permits high efficiency for observing the 0.5 MeV γ's produced by annihilation in $\bar{\nu}p$ events. These two regions are, in turn, surrounded by an oil "buffer" in which the phototubes are immersed. The buffer region extends to a 290 cm radius to allow movement of the detector within the 300 cm radius tunnel. Hence the buffer is 70 cm in thickness and phototubes are located about 100 cm from the central region or 140 cm from the fiducial region.

Given this layout, the fiducial volume of each detector is 13 tons. Therefore, two near detectors are required to attain the necessary statistics. This is consistent with the Braidwood design.

2.1.1 Response to Reactor-induced Events

The goal of the detector is to identify and count the two types of reactor-induced events: elastic scattering and inverse beta decay. In order to do this, accurate energy and vertex reconstruction are required. Also, it is necessary to identify neutrons produced in inverse beta decay with high efficiency. It is worth noting that, for this analysis, it is not necessary to reconstruct the angle of the outgoing lepton. This is in keeping with the detector design, where the the high level of scintillation light will obscure any directional Cerenkov light.

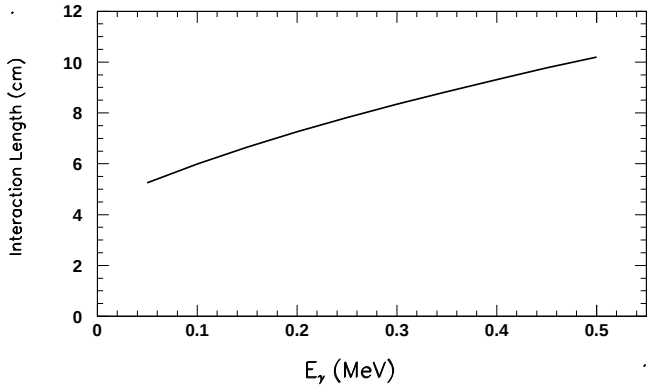

Figure 5: Compton length as a function of photon energy.

The two types of events have different visible energy distributions, as shown in Fig. 3. In order to be able to relate the rates for the two processes, one needs a good understanding of the energy resolution. An energy resolution of $\leq 10\%$ appears to be attainable. CHOOZ achieved an energy resolution of 0.33 MeV at 8.1 MeV [6]. The CTF detector used α-decays with a corresponding electron-like energy of 862 keV to show that, in the central region of the detector, energy resolution of 4-5% is attainable [12]. The KamLAND detector has reported $\sim 7.5\%/\sqrt{E(MeV)}$ energy resolution [13]. In section 6, we show that systematics on smearing due to energy resolution leads to a negligible systematic error in the analysis.

To obtain good energy resolution for the normalization sample, the annihilation photons in inverse beta decay events must be contained. These photons lose energy through Compton scatters, with a path length that depends on energy, and in CH_2, is ~ 11 cm (see Fig. 5). While the Compton peak is at $2/3E_\gamma$, note that the average energy loss is $1/3E_\gamma$. Thus an event can be expected to have several Compton scatters before exiting the detector. The "photon catcher" region and outer 40 cm of the Gd-doped region

are used to contain and reconstruct the energy of these photons. The 1.5 m radius fiducial volume cut places a 0.5 MeV photon at approximately 6.5 path lengths from the inactive oil-buffer region. The result is negligible loss due to a photon escaping.

We do not consider smearing due to vertex resolution at the edge of the fiducial region. To a good approximation, the vertex resolution is the same for the $\bar{\nu}e$ signal and $\bar{\nu}p$ normalization events. Hence, the systematics related to vertex resolution should cancel. However, we note that good vertex resolution is important for identifying and removing backgrounds. We believe that $\sim$4 cm on the interaction vertex may be attainable. This is consistent with CHOOZ laser flasher studies [6]. CTF obtained a similar resolution using an alpha source, corresponding to a photon energy of 0.862 MeV [12]. This is sufficiently good that we believe vertex resolution issues will be a small effect in the final analysis and are not considered further here.

In order to identify $\bar{\nu}p$ events, which represent both a background and a normalization sample, the signal from the neutron capture is used. In Gd-doped scintillator, a typical separation length from neutrino vertex to neutron capture is 6 cm, as measured in CHOOZ [6]. Therefore, the fiducial volume cut of 40 cm from the central region edge represents 6.7 separation lengths. Only a small fraction of the n's are produced at the edge of the fiducial region, and of those, only about half drift outward. Folding in the geometry, assuming a uniform distribution for neutron production throughout the tank, 1.1×10^{-5} neutrons will exit without capturing. This contribution to the background will be considered further in section 4.

Neutron capture is time-delayed with respect to the positron track, with a capture time of 30.5 μs measured in CHOOZ [6]. Using this as our baseline, we assume a time window of $0.5 < \Delta t < 200\mu$s, which is wider then the CHOOZ neutron delay time window. Based on our Monte Carlo (see section 2.4), this results in 0.1% failures in associating a neutrino vertex due to early captures and 0.1% failures due to late captures. We will address how these events can be removed in section 4.

Gd-doping results in a cascade of photons resulting in 5.6 to 8 MeV when the neutron captures, depending on the Gd isotope. The dominant cross sections are for ^{155}Gd and ^{157}Gd, both of which result in $\sim$ 8 MeV of released energy. The remaining Gd isotopes represent $< 9 \times 10^{-5}$ of all Gd captures. Those which released less than 6 MeV (^{158}Gd and ^{160}Gd) represented only 1.4×10^{-5} of all Gd captures. Therefore we assume that the reconstructed energy for n captures on Gd is always > 5 MeV. Due to the excellent energy

resolution, we will assume that 100% of these captures are observed.

CHOOZ found that the percentage of events which capture on Gd is 84% [6]. We will use this capture fraction in our calculations. To increase the probability of Gd capture, as well as assure that the reconstructed energy is always > 5 MeV, it may be preferable to use isotopically-enhanced Gd. This has not been done in past experiments and requires further investigation.

The remaining 16% of neutrons will capture on hydrogen, resulting in a single 2.2 MeV γ. In this analysis, it is necessary for a large fraction of these events to be identified using a combination of timing and position. CHOOZ studied a trigger[14] for the H capture events, but this was developed late in the experiment and not implemented before data taking ended. However, the initial results looked promising. KamLAND quotes an efficiency for $\bar{\nu}p$ events of 78$\pm$1.6%[13]. This experiment is performed on oil with no Gd-doping, thus the n path length is large. The inefficiency is largely driven by the cut on relative position of the neutrino and neutron vertex. In order to proceed with background calculations, we assume a search window of 30 cm or five neutron path lengths will be feasible. This yields a 0.6% inefficiency due to neutrons which exit the window, which we will consider in section 4. It is desirable to make this window larger, if the trigger rate can be tolerated.

2.1.2 Measuring the Gd and H Capture Fractions

CHOOZ measured the capture fraction on Gd to 1% error using a radioactive "Am/Be" source. The decay chains associated with this source are:

$$^{241}\mathrm{Am} \rightarrow ^{237}\mathrm{Np}+\alpha;\ \alpha+^{9}\mathrm{Be}\rightarrow ^{12}\mathrm{C}^{*}+n;\ ^{12}\mathrm{C}^{*} \rightarrow ^{12}\mathrm{C}+\gamma\ (4.4\ \mathrm{MeV}).$$

Thus, this source produces γ's in conjunction with a neutron allowing a coincidence signal to be measured. Because this experiment will run for three times the CHOOZ period, and because the Gd capture fraction can be measured in both near detectors and the four far detectors (see section 2.2), more than an order of magnitude more calibration data will be collected. Thus, in principle, the Gd capture fraction can be measured to better than 0.25%.

As additional assurance that the capture fraction can be measured well, we propose a small, dedicated detector with excellent energy resolution to accurately measure the fraction of Gd captures. The detector must have excellent energy resolution assuring a clean separation between the H capture

energy peak and the Gd capture energy peak. The detector will consist of Gd doped scintillator which is of the same batch as the near and far detectors. A permanently installed Am/Be source would provide the trigger. One would want the fiducial radius to be at least six neutron path lengths, or 36 cm. It need not be a miniature version of the near detector – in fact other designs may be preferable and easy to obtain. For example, the SciBath detector design proposed by the FINeSSE experiment could be used for this purpose [15].

2.1.3 Contamination in the Detector

As discussed in section 1, the main decay chain of concern is ^{232}Th. We will show in section 5 that the fiducial volume cut reduces the background from the tank walls, phototubes, and acrylic vessel to a negligible level. Nevertheless, precautions at the level of KamLAND should be taken with these components.

The most important contamination issue is the amount of Th dissolved in the oil. A small fraction of the daughters in the ^{238}U decay chain also produce visible energy in the 3 to 5 MeV region. Other radioactive contaminants, such as K and ^{14}C are not considered because the visible energy from these decays is below the energy level of this study. Because the four far detectors will be used to study contaminants, all detectors should be filled with oil from the same batch to assure similar purity.

Our goal is to achieve the same fractional Th concentration in the scintillator as has been achieved at KamLAND [9], which is 5×10^{-17} g/g. While we will show in section 7.3 that two orders of magnitude higher contamination can be tolerated if necessary, KamLAND level purity is undoubtedly desirable. Reaching this level of purity requires addressing the cleanliness of the scintillator oil and also the contamination of the Gd-dopant. Purifying scintillator to attain low levels of dissolved thorium is has been demonstrated. At the CTF experiment, the scintillator was delivered from the refinery with a purity of $4.4 \pm 1.4 \times 10^{-16}$ g/g of ^{232}Th [16]. Further purification at the detector site reduced the level to $< 2 \times 10^{-16}$ [16]. Similarly, KamLAND quotes a level of 5.2×10^{-17} g/g of dissolved ^{232}Th [9]. On the other hand, additional study is needed to assure the required purity of the Gd, which is isolated from contaminants by an evaporation process. For the discussion below we will assume that 5×10^{-17} g/g of ^{232}Th is attained in the detector, although we will show that 100 times this rate can be tolerated.

Our goal for ^{238}U contamination is the KamLAND level of 3.5×10^{-18} g/g [9]. This is consistent with the CTF level, which is reported as $< 1 \times 10^{-17}$ g/g [16]. Similar to the case of ^{232}Th, CTF reports that the delivery from the refinery was already very pure with $< 1 \times 10^{-16}$ g/g. Thus achieving these levels with modest additional purification appears practical. Again, the issue of contamination of the Gd must be addressed to achieve these goals.

2.1.4 Cosmic Ray Identification Systems

As described in section 1, cosmic ray background must be reduced for this analysis. We assume the detector overburden to be 300 mwe, which yielded a cosmic ray flux, based on our calculation, of $0.5/\mathrm{m}^2/\mathrm{s}$. Given the proposed generic design, which has two detectors each with a 1.5 m radius of active area for cosmic rays, the rate will be 3.5 Hz per detector.

For the oscillation experiment, most designs propose an active veto region which surrounds the detector [17]. This can be designed with at least $>$ 99.99% efficiency as achieved in MiniBooNE [18]. We recommend that the veto be constructed with segmentation, so that the direction of the cosmic ray can be determined.

However, for this analysis, an upper/side veto is not sufficient. Therefore, we propose to use the detector itself for highly efficient cosmic ray identification. We can place the detector in a logical "or" with the active veto if even further efficiency is necessary; we believe, however, that this is unlikely. In order to discuss the algorithm for identifying cosmic rays in the tank, we will assume that 200 photoelectrons per MeV are detected. This rate of photoelectrons per MeV is similar to the CHOOZ design[6] and is one third less than the Borexino test detector, CTF [19]. It is more than sufficient for our needs here.

We identify cosmic rays in the detector using the fact that they are the unique source of events above the cutoff of Michel electrons (about 52 MeV). Cosmic ray muons deposit about 2 MeV/cm [18, 20]. Assuming the same level in this detector, this yields 0.4 hits/cm/phototube for muons which radially traverse the photon catcher. For this analysis, we are interested in muons which penetrate into the fiducial volume. To penetrate into the fiducial region, the muons must pass through a minimum of 70 cm of scintillator, depositing 140 MeV of energy in this model, well above the Michel electron cutoff. We will call a muon with $E > 140$ MeV a "penetrating μ" for the remainder of the discussion.

The need to simultaneously reconstruct reactor-induced events and penetrating μ's implies that the electronics must be sufficient to reconstruct events which range from 1 MeV to at least 140 MeV. Ability to resolve energies above 140 MeV is desirable, since it will allow better understanding of the cosmic rays. With 200 PE/MeV and 1000 phototubes, 140 MeV represents 28 PE/phototube (where PE means photoelectrons). Thus, the electronics requires a minimum dynamic range of at least a factor of $\sim$30 (*i.e.* from 1 PE to more than 28 PE) without saturation, and larger would be better. Electronics used in SNO [21] had a dynamic range of 1 to 1000 PE, so a substantially larger range is certainly possible.

An additional "lower veto system" will be installed under the detector. This system will be used in anti-coincidence with a cosmic signal in the detector to select events where the muon stopped in the detector. This will reduce the rate of potential parent cosmic rays for the ^{12}B search to an acceptable level. We recommend that this scintillator be segmented, so that when used in conjunction with the upper/side veto, the cosmic ray track direction can be reconstructed to within a few centimeters. This also reduces false coincidence rates.

2.2 Construction of the Far Detectors

We will show in section 5.5.2 that if care is taken to make the far detectors as identical as possible to the near detectors, they can perform a crucial role in constraining backgrounds. They are also useful for gaining statistics on the Gd capture fraction using the the Am/Be source, as discussed above. All present designs for the proposed oscillation measurement call for several near and far detectors [7] and here we assume there are four. For our arguments, we take them to be located at 1.8 km from the reactor cores, with the same construction conditions and materials and detector hall as the near detectors. We believe that the most difficult variable to control will be the thickness of overburden, even within a flat environment such as Braidwood.

2.3 The Standard Cuts

Based on the detector described above, we propose a set of "standard" analysis cuts. These will be used to evaluate the capability of the experiment. There are two event samples relevant to the analysis. The elastic scattering signal sample, which has a single e^- and the inverse beta decay normalization

Cuts, all samples	**Range Retained**	**Primary Motivation**
Fiducial volume	45 cm inward from Gd boundary	maintain high n efficiency.
Vetoes, all samples	**Description**	**Primary Motivation**
Stopping Muon Veto	No lower veto hit & penetrating μ; veto window: 200 ms	vetoes ^{12}B and Michel backgrounds (deadtime: 1.5%)
Muon-neutron veto	Penetrating μ followed by neutron signal within 600 ms; veto window: 3s	vetoes isotopes which β-decay (deadtime: 6.4%)
Cuts, elastic scattering sample	**Range Retained**	**Primary Motivation**
Minimum visible energy Maximum visible energy	> 3 MeV < 5 MeV	Reduce all sources of backgrounds
Neutron capture energy & delay window	$< 1.8 MeV$ in $0.5 < \Delta T < 200 \mu$s	identify and cut $\bar{\nu}p$
Cuts, normalization sample	**Range Retained**	**Primary Motivation**
Neutron capture energy & delay window	$E > 5$ MeV $0.5 < \Delta T < 200 \mu$s	Isolate well-identified events to maximize n id purity
Minimum visible energy	> 2.2 MeV	isolate events with flux which overlaps $\bar{\nu}e$ signal

Table 4: General motivation for the major cuts. "Elastic" and "Normalization" samples are described in section 1. Visible energy refers to the measured energy of the primary interaction.

sample, which has $e^+ + n$ in the final state. The cuts fall into four categories: cuts applied to both event samples; vetoes applied to all event samples; cuts applied to isolate the elastic scattering sample; and cuts applied to isolate the normalization sample. The standard cuts on which we will base our estimate for the error on $\sin^2\theta_W$ are listed in Table 4.

2.3.1 Overview of Analysis Level Vetoes

Two analysis-level vetoes are employed: the stopped muon veto and the muon-neutron veto. The first veto is designed to reduce background from Michel electrons and ^{12}B beta-decays. The second removes high-energy-muon-induced β-decaying isotopes. Note that neither veto requires the presence of a signal candidate. This is because the deadtime induced by the veto must be the same for the signal and normalization samples. We thereby avoid a significant systematic associated with understanding the deadtime.

The stopped muon veto is applied in the following way. The presence of a "stopped muon" is identified by requiring a penetrating μ in coincidence with no signal in the lower veto system. All subsequent events in a 200 ms window are then eliminated. The 200 ms window was chosen because it is about ten ^{12}B lifetimes and thousands of muon-decay lifetimes. It thereby successfully eliminates these backgrounds.

For this discussion, we will assume the stopped muon veto is 100% efficient. Inefficiency in identifying the muon signal could cause this veto to fail. However, this is expected to be negligible, as discussed above. Inefficiency in the lower veto increases the deadtime, as discussed below, but does not cause the veto to fail. Noise in the lower veto in coincidence with a stopping cosmic could cause the veto to fail. But a combination of selecting quiet phototubes and segmented construction can reduce this to a negligible level.

The muon-neutron veto removes all events which follow a muon-neutron signal within a 3 s period. The purpose is to reduce the background from muon-induced β-decaying isotopes produced in conjunction with neutrons (see Table 1). The muon-neutron signal is defined as a penetrating μ followed by at least one neutron signal in the central region. Neutron signals for this veto are defined as clusters in time of 6 to 10 MeV signals, which occur within a total window $0.5 < \Delta t < 600$ μs after the muon has penetrated the fiducial volume. The number of these clusters is simply counted.

The efficiency of the muon-neutron veto is driven by the ability to identify the neutrons. Inefficiency occurs when the neutron exits or when the neutron

fails to capture on Gd. Because of the later requirement, which is introduced to assure the veto has a low rate of random coincidences, the maximum possible efficiency per neutron is 84% (the Gd capture fraction). This is not a major issue for the isotopes where three neutrons are produced, but it does represent a substantial inefficiency for ^{8}Li, where only one neutron is produced. Thus, if the rate of H-capture-like events is sufficiently small, one would want to include these also. This is not assumed at present, however.

The probability that a neutron will escape depends on the position where it was produced and its initial energy. We are interested in the case where the muon-interaction vertex occurred in the signal region. In this case, the neutron must traverse a minimum of 40 cm of Gd before it can exit the central region. We find that 81% of the neutrons produced by spallation traverse $\leq$ 40 cm. Thus, 19% represents a gross upper limit on the expected inefficiency for neutron captures from spallation. We will use this in calculations related to the muon-neutron veto. In order to assure a low rate from accidental coincidences, we will only veto on events where at least one neutron captures on Gd. Hence the lower limit on the total efficiency is given by 81% $\times$ 84% (the Gd capture fraction), or 68% per neutron. For three neutrons, the veto will be $>$ 97% efficient.

2.3.2 Deadtime Induced by the Vetoes

Deadtime is not a major consideration in this analysis because the signal and normalization samples will be equally affected by the vetoes. Nevertheless, when one is doing a precision measurement, as a matter of practice it is best to have the lowest possible deadtime. Also, one aims for a small deadtime so that one can run for the minimum possible time. In considering the discussion below, note that a veto which depended only on the presence of a cosmic ray, without asking for a stopping signal or accompanying neutrons, would lead to intolerable deadtimes.

The deadtime for the stopped muon veto will be 0.84% given the expected stopped muon rate 0.042 Hz. This is acceptable. In principle, inefficiency in the lower veto could produce misidentified stopping muons. It is reasonable to assume that this veto can be made better than 99% efficient. Assuming a 1% inefficiency would lead to a deadtime of only 1.5% (veto inefficiency and real stopped muon rate, combined). This is sufficiently small to not be an issue.

Note that if we had not introduced the lower veto, and simply used all

incoming muons, the deadtime, assuming a 3.5 Hz rate, would have been 70%. This is far too high. Thus the lower veto system is necessary for a veto system which can remove ^{12}B as well as Michel electron events.

To calculate the rate at which the muon-neutron veto will fire, one needs to consider both the muon signal rate and the neutron signal rate. To estimate the neutron rate, we use a simulation which is described below in section 2.4. We expect 0.042 muon-induced neutrons/s (or 3650 neutrons/d). However, we note that many of these neutrons will be produced simultaneously by the same parent cosmic muon. Thus this represents a gross upper estimate. In order to correct for multiple neutron production, we assume an average multiplicity of two, consistent with the result of reference [22]. Thus we take as our prediction a rate of 0.022 Hz. Opening a 3 s window, thereby introduces a 6.4% deadtime. This is an acceptable rate and is probably an overestimate. In fact, to further reduce backgrounds from β-decaying isotopes, one might consider enlarging this window.

To address the rate of accidental firing of this veto, we must consider the types of events which can cause each component to fire. The cosmic signal is unique among the types of events which can occur, due to the very high energy. Therefore, we assume that there is no accidental background within this component. The most likely false vetoes come from Michel electrons and ^{12}B decays, because these events are correlated to an incoming muon. Neutrons which enter the tank can also produce a muon-neutron coincidence. This rate is much lower, however, because the neutron and cosmic ray are not correlated, and so we do not consider this here.

The largest contribution to the accidental muon-neutron coincidence is stopped cosmics plus Michel electrons which fake the neutron-component. Given the 2.2 μs lifetime of a muon, the time window for the neutron search, which opens 500 ns after the muon, eliminates 20% of the Michel electrons. In order to estimate the number of Michel electrons in the 6 to 10 MeV range, we assume a flat distribution. The result is that 8% fall within this range. This is clearly an overestimate since the true distribution peaks near the 52 MeV endpoint. Combining these requirements, $\sim$ 6% of the Michel electrons are within 6 to 10 MeV thereby faking a neutron signal. The rate of stopped muons is 0.042 Hz. Thus the rate of cosmic+Michel fulfilling the muon-neutron component is 0.003 Hz, which is much smaller than the true muon-neutron signal.

^{12}B decays will contribute at about half the rate from Michel electrons to the muon-neutron veto. Only 8% of the stopping μ^-'s capture to produce

^{12}B. Less than half of the electrons produced by ^{12}B decays fall within the energy range for a neutron.

2.4 Calculation of Neutron Production and Transport

The above discussion and that which follows relies on a high quality Monte Carlo description of the interactions of cosmic rays at a depth of ~ 300 mwe. To calculate the production of fast neutrons by cosmic ray muons at depth, we begin with a parameterization of muon rate at the surface as a function of energy and zenith angle [23]. The muon rate is divided into 750,000 bins in energy (100 MeV steps from 0 to 2.5 TeV) and angle (2° steps from 0° to 60°). In each bin the energy is attenuated in steps of one meter (larger steps are used for very high energies) according to the average energy loss as a function of muon energy [20]. Given the muon rate and spectrum at depth, we use the neutron production model of Wang *et al.* [24] to determine the neutron spectrum at rate. Similarly, the isotope production is determined using the normalization and energy scaling of Hagner *et al.* [10].

The neutron transport Monte Carlo takes the neutron production energy distribution as an input, and propagates the neutrons assuming elastic scattering in CH_2 with 0.1% Gd by weight. The cross sections for elastic scattering and capture on H, C, and Gd are taken from reference [25].

3 $\bar{\nu}e$ Event Rate and Identification

$\bar{\nu}e$ events result either from scattering via exchange of a Z boson, or annihilation via exchange of a W boson. The differential cross section for $\overline{\nu}_e e^-$ scattering is:

$$\frac{d\sigma}{dT} = \frac{G_F^2 m_e}{2\pi}\left[(g_V+g_A)^2+(g_V-g_A)^2\left(1-\frac{T}{E_\nu}\right)^2+(g_A^2-g_V^2)\frac{m_e T}{E_\nu^2}\right] + \frac{\pi\alpha^2\mu_e^2}{m_e^2}\frac{(1-T/E_\nu)}{T}$$

where E_ν is the incident $\overline{\nu}_e$ energy, T the electron recoil kinetic energy, and the couplings are given by

$$g_V = 2\sin^2\theta_W + \frac{1}{2} \qquad g_A = -\frac{1}{2}$$

The term in brackets is the weak interaction contribution, and the last term gives the contribution from electromagnetic scattering if the neutrino has a magnetic moment, μ_e.

The total visible energy, E_{vis} in elastic scatters is the kinetic energy of the e^-, T. This is in contrast to $\bar{\nu}p$ events where additional visible energy will come from both the positron annihilation and the neutron capture.

If one could reconstruct both T and E_ν in $\bar{\nu}e$ events, then an analysis of T/E_ν dependence would be attractive. This method evades the issue of absolute normalization. However, in the generic detector described above the angle of the e^- cannot be reconstructed. Therefore, only T is measurable. Once this cross section is folded with the reactor flux, the variation of the shape versus T is insensitive to $\sin^2\theta_W$.

On the other hand, the total rate of $\bar{\nu}$ events is sensitive to $\sin^2\theta_W$. In fact, the sensitivity to $\sin^2\theta_W$ can be enhanced by introducing a cut on T. Integrating over the recoil electron kinetic energy from $T_{\min}$ to $T_{\max}$ gives a cross section as a function of E_ν given by

$$\begin{aligned}\sigma_{T_{\min}\text{ to }T_{\max}} &= \tfrac{G_F^2 m_e}{2\pi}\Big[\left((g_V+g_A)^2+(g_V-g_A)^2\right)(T_{\max}-T_{\min}) \\ &\quad +\tfrac{1}{2}\left(\tfrac{m_e\left(g_A^2-g_V^2\right)}{E_\nu^2}-\tfrac{2(g_V-g_A)^2}{E_\nu}\right)(T_{\max}^2-T_{\min}^2) \\ &\quad +\tfrac{(g_V-g_A)^2}{3E_\nu^2}(T_{\max}^3-T_{\min}^3)\Big]\end{aligned}$$

T in the range of 2.5 to 5 MeV is optimal. As discussed in section 1, however, cuts on various backgrounds dictate $3 < (T = E_{vis}) < 5$ MeV.

We assume that the term associated with the neutrino magnetic moment (μ_e) is negligible, based on astrophysical constraints [26, 27, 28, 29]. A neutrino magnetic moment enhances neutrino pair production. This will affect the cooling of red giants, delaying He ignition. The resulting limit is $\sim 3\times10^{-12}$, and appears to be robust against model dependences. The magnetic moment also affects pair-production in supernovae. While this result may have more model dependence, the limit is similar to that obtained from observation of red giants. We note, though, that the lab-based limits on the neutrino magnetic moment are two orders of magnitude higher [8]. If, for some reason, the astrophysical constraints were proved to be unjustified, and if the neutrino magnetic moment were just below the lab-based limit (e.g. 10^{-10}), then this term would result in a 12% increase in the elastic scattering rate.

4 The $\bar{\nu}p$ Background

A major potential source of background comes from misidentified $\overline{\nu}_e p \rightarrow e^+ n$ events. The cross section is given by

$$\sigma\left(E_{e^+}\right) = \frac{2\pi^2}{m_e^5 f \tau_n} p_{e^+} E_{e^+}$$

where $E_{e^+}(p_{e^+})$ is the energy(momentum) of the outgoing positron, $f = 1.71465(15)$ [11, 6] is the free neutron decay phase-space factor, and $\tau_n = 886.7 \pm 1.9$ s [30] is the neutron lifetime. Using these measurements of f and τ_n, one finds that the cross section is known to the 0.2% level. The cross section is therefore very well known. For this process, the $E_{\overline{\nu}_e}$ energy threshold is 1.804 MeV and the incoming $\overline{\nu}_e$ energy is simply related to the outgoing positron energy by

$$E_{\overline{\nu}} = E_{e^+} + (M_n - M_p) = E_{e^+} + 1.2933 \text{ MeV} .$$

Most $\bar{\nu}p \rightarrow e^+ n$ are identified by the outgoing n. The n may not be observed, however, because of the the inefficiency on triggering on H capture, or because the neutron was outside of the neutron-delay time window. In the latter case, 0.1% of the neutron capture signals occur early and will be included in the visible energy associated with the neutrino vertex. Also, 0.1% of the neutrons will capture late, leaving a primary neutrino vertex and a secondary neutron vertex which is mistakenly "unassociated." Requiring that these events have reconstructed energy within the E_{vis} window, however, reduces the rates further.

4.1 Rejection through n Identification

Most $\bar{\nu}p$ events can be rejected through identification of the time-delayed n. We take the efficiency for reconstructing the photons from Gd capture to be 100%. On the other hand, the efficiency for identifying the photon associated with H capture is only 99.4%. Thus the total n-identification efficiency is $0.84 + (0.16 \times 0.994) = 0.999$. This is to say, 0.1% of n events within the neutron time window will fail to be identified.

The systematic error on this is small. The error on the Gd capture fraction is assumed to be 0.3% (see section 2). The Gd capture fraction introduces an error, δ, which changes the efficiency to $\epsilon = (0.84 + \delta) + (0.16 - \delta) \times 0.994$.

Taking the derivative, $d\epsilon = .006 d\delta$. Assuming we can indeed measure δ to 0.003, the result is an error of 2×10^{-5}. The 0.006 inefficiency on H capture comes from neutrons which exit the 30 cm search region. In this case, using binomial statistics, one needs 17,000 tagged calibration-source events in order to obtain a 10% error on this inefficiency. This should be achievable using the *in situ* Am/Be source calibration. We therefore assume no systematic error contribution from this source.

4.2 Rejection through an E_{vis} Cut

There are four cases where the neutron is "lost" to the analysis. First, the neutron capture occurs earlier than the neutron delay time window in 0.1% of the $\bar{\nu}p$ cases. Second, 0.1% of the time the neutron captures is sufficiently late that it is outside of the time window. Third, 0.0011% of the $\bar{\nu}p$ interactions, neutrons exit the Gd-doped central region without capturing. Fourth, for 0.1% of the $\bar{\nu}p$ events, the neutron fails to capture within the H-trigger spatially allowed range (see section 2.1.1). All of these backgrounds are further reduced by the E_{vis} cut.

There is one case where the neutron is not identified in the triggering, but the energy due to the neutron is still associated with the event. This is the case of early captures, where the neutron fails to fall within the time-window. First, consider the case of early captures on Gd. These will deposit ~ 8 MeV, which falls outside of the visible energy window. Next, consider the case of the 16% of events with an early capture on H. In these events the neutron releases 2.2 MeV and the positron annihilation releases 1 MeV. Thus the minimum visible energy for $\bar{\nu}p$ with H capture is 3.2 MeV. Events with up to 1.8 MeV in positron kinetic energy will be within the visible energy window. 20% of $\bar{\nu}p$ events will have positron kinetic energy in this range. This 0.1% background is therefore reduced by the factor 0.16×0.20 to 0.003% of the $\bar{\nu}p$ interactions. We again assume the systematic error on this is sufficiently small to be neglected in this discussion.

In the cases where the neutron captures late, exits the central region, or captures on H outside of the H-trigger search region, only the neutrino vertex energy is observed. The total visible energy for an unassociated positron is the kinetic energy of the lepton plus 1 MeV from the positron annihilation. Approximately 60% of the unassociated positron events fall within the $3 < E_{vis} < 5$ MeV window. The background for late captures is therefore reduced to 0.06%. The fraction of events with neutrons which exit and with neutrino

vertex energy within the window is 7×10^{-6}. The case where the neutron is lost from the H-trigger search region, follows the same argument. This background source therefore drops to 0.06% of the $\bar{\nu}p$ events. Again we assume no appreciable systematic error on these values.

4.3 Unassociated (Late) Neutrons

In the 0.1% of $\bar{\nu}p$ events, where the neutron capture is late, the unassociated neutron could potentially produce a background. In this case, the neutron will not be properly associated with the neutrino vertex. These unassociated neutrons will appear to be a single vertex. However, those which capture on H will produce a 2.2 MeV γ and those which capture on Gd will produce > 8 MeV visible energy. Therefore, the background from unassociated neutrons will be negligible.

4.4 Summary of $\bar{\nu}p$ Backgrounds

Four sources of events that contribute more than 10 events to the $\bar{\nu}p$ backgrounds are identified. The fractional contributions, in order of importance, are:

1. Events with a late neutron capture, thus having an unassociated positron vertex: 6×10^{-4}.

2. Events in the neutron delay time window which fail to have a reconstructed capture: 6×10^{-4}.

3. Events with an early neutron capture that were not eliminated through the $E_{vis\ max}$ cut: 3×10^{-5}.

4. Events with a neutron which exits and which were not eliminated through the $E_{vis\ max}$ cut: 7×10^{-6}.

Based on this, we take the the total $\bar{\nu}p$ background to be estimated as 0.12% of the $\bar{\nu}p$ interactions. The systematic error on this is considered to be negligible. Within the $3 < E_{vis} < 5$ MeV window, we assume that $\bar{\nu}e$ reconstruction is 100% efficient.

5 Environmental Backgrounds

Section 1 introduced the environmental backgrounds which reactor experiments face. Potentially, they come from contaminants, cosmic ray muons, and products of cosmic ray muons such as Michel electrons, spallation neutrons, and muon-produced isotopes. We assume cosmic muons are readily identifiable, as described in section 2.1.4. We show that the $3 < E_{vis} < 5$ MeV window, in combination with the vetoes proposed in section 2.3.1, reduce most environmental backgrounds to a negligible level. ^{232}Th is the most important contaminant chain. Muon-produced isotopes will represent the largest environmental background.

In principle, solar neutrinos represent an environmental background. As calculated by reference [31], the background from solar neutrino interaction is small. The rate for the flux between 3 to 5 MeV, which is expected to be dominated by the ^{8}B solar neutrinos, is 4 events in the 900 day run. Atmospheric neutrino rates are considerably lower than solar neutrino rates, and so these, too, can be neglected.

Also, geoneutrinos from β-decays in the core of the earth, which have energies < 3.5 MeV are not an issue in this analysis. First, the rate is expected to be very small. Second, the geoneutrinos are actually antineutrinos, and they will contribute commensurately to both the elastic scattering signal mode and the inverse beta decay normalizing mode.

5.1 Backgrounds from Radioactive Contaminants

Decays of radioactive contaminants may produce background in the analysis. As an example of what can be expected, Fig. 4 shows the singles rate as a function of visible energy within the inner 5 m radius of the KamLAND detector. The expectation for decays of radioactive elements are also shown on the plot. In the 3 to 5 MeV window, the main contribution is from the ^{232}Th chain. Compared to the Th contribution, there is a $< 5\%$ contribution from the ^{238}U chain, which is isolated to < 3.5 MeV.

We assume for this analysis that levels of purity similar to those achieved at KamLAND and CTF can be attained by this experiment. An important difference between this experiment and KamLAND is the Gd doping. We will assume that the Gd dopant can be purified of U and Th to a level similar to the oil. In section 7, however, we consider the effect if the U and Th levels are substantially higher than KamLAND.

5.1.1 The ^{232}Th decay chain

The decay chain for ^{232}Th is shown in Fig. 6. The half life for each step is also listed in the figure.

The ^{232}Th chain produces six alpha particles of energy 4 to 9 MeV. Scintillation signals quench by factor of 10 to 15, so each alpha deposits roughly 0.25 to 0.8 MeV in the detector. It is highly unlikely that multiple decays will occur simultaneously, thus the α's do not represent a background.

Five β's are also produced in the decay chain, and the respective energies of the β's are listed on Fig. 6. The issue for this analysis is the decay of ^{208}Tl to ^{208}Pb. This releases a β with energy up to 1.8 MeV and, simultaneously, γ's, including a 2.4 MeV γ. The total energy of this decay is 5 MeV. Therefore this decay has sufficient endpoint energy to appear in the $3 < E_{vis} < 5$ MeV window. Luckily, this decay lies along a branch of the the chain, so only 35% of the parent ^{232}Th will produce this background.

The Th-related contaminants on the acrylic balloon will not be a background because the events will be removed by the fiducial volume requirement for this analysis. The γ's produced by this decay chain, which will enter the fiducial volume, are below the 3 MeV visible energy window, which means that they do not contribute. This leaves the dissolved ^{232}Th in the scintillator as the main issue.

We calculate the contribution to the background from ^{232}Th assuming 5×10^{-17} g/g. In 13×10^6 g per detector, there is 6.5×10^{-10} g of ^{232}Th per detector. The mass is 232 g/mol; thus we have about 3×10^{-12} moles or about 1.75×10^{12} ^{232}Th isotopes/detector. The half-life is 1.4×10^{10} years, yielding 265 events decay during the run. We double this for two detectors to obtain 530 events. We then take 35% for the branching of ^{208}Tl to ^{208}Pb, to obtain 185 events. These events will be reconstructed with the combined energy of the emitted γ and the β. Combining these energies, we find that 51% are expected to reconstruct within the 3 to 5 MeV window. The total is therefore 93 events in the two near detectors.

5.1.2 The ^{238}U Chain

As seen in Fig. 4, there are also a small fraction of background events, from 3 to 3.5 MeV, which are due to the ^{238}U chain. These events are produced from a β decay within this chain with an endpoint of 3.2 MeV. We will assume that we can achieve the same level of uranium contamination as KamLAND.

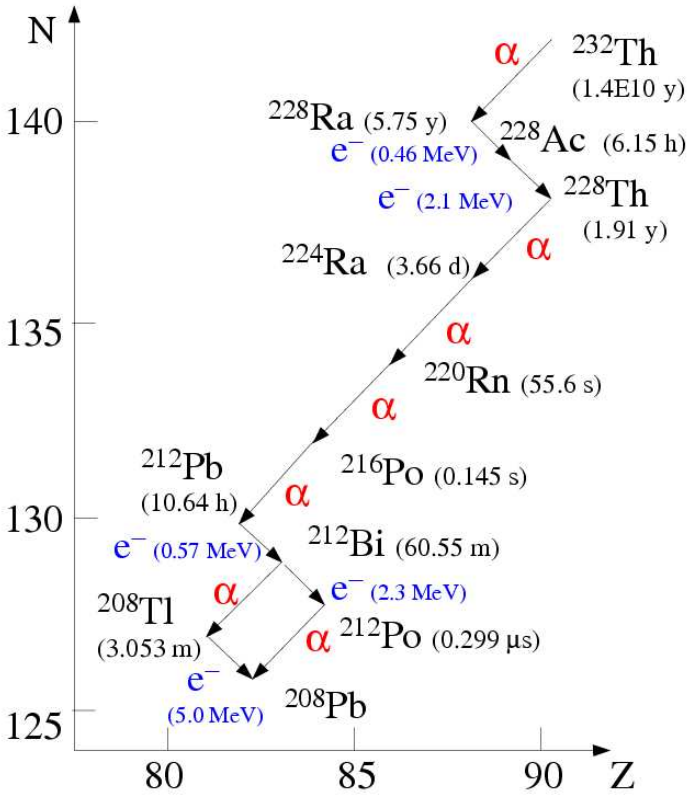

Figure 6: Decay chain for ^{238}Th. Half-life of each step is listed in parentheses. For β decays, the total visible energy released (β's and γ's) is noted.

Judging from Fig. 4, the U contribution in the visible energy window is only about 5% of the Th contribution, or about 5 events for the two near detectors combined.

5.1.3 How Well Can We Measure these Backgrounds?

The systematic error on this background can be determined by two methods, one relying on external measurement and the other relying on the far detectors. In the first method, samples of the oil will be studied in a low background counting facility located deep underground. This will allow an absolute measure of the β decay of concern which can be quite precise. However, it relies on Monte Carlo to accurately represent the smearing. In the second method, we use the far detectors to measure the background in the visible energy window of the near detector. This method is discussed in section 5.5.2 and is expected to predict the rates in the near detector in the visible energy window for all environmental sources, including the U and Th contributions, to about 50 events.

5.2 Michel Electron Background

The ratio of stopping to through-going muons at 300 mwe has been calculated to be 6×10^{-3}/m [32]. The flux of cosmic rays entering a detector under 300 mwe overburden is 0.5 $\mu/\mathrm{m}^2/\mathrm{s}$. The stopping rate in the detector is therefore $0.003/\mathrm{m}^3/\mathrm{s}$. The fiducial region of the generic detector is 1.5 m, thus the stopping rate is 0.042 Hz, or about 3.3×10^6 Michel decays for the run, per detector.

The stopped muon veto represents many thousands of muon lifetimes. Hence, we will assume that all Michel electrons are removed as background. On the other hand, Michel electrons represent a well-identified control sample for studies in this analysis. If all detectors are built identically, then the Michel samples can be combined, greatly enhancing these studies.

5.3 Neutrons

Cosmic rays can produce spallation neutrons either outside or within the tank, but these are a negligible background. This is because these neutrons, like unassociated neutrons described above, will fail the energy window. H captures result in a visible energy which is below 3 MeV, and Gd

Isotope	1/2 life (s)	Endpoint (MeV)	Rate/ton (1/t/d)	Rate/detector (1/d)
^{9}Li+^{8}He	0.18 & 0.12	13.6 & 10.6	0.15±0.02	1.95±0.26
^{8}Li	0.84	16.0	0.28±0.11	3.64±1.43
^{6}He	0.81	3.5	1.1±0.2	14.70±2.60
^{9}C	0.13	16.0	0.34±0.11	4.42±1.43
^{8}B	0.77	13.7	0.50±0.12	6.50±1.56

Table 5: Isotopes with energy endpoint > 3 MeV. Rate/detector/day is for the generic 13 ton detector under 300 mwe overburden. Top table: β^- production; bottom table: β^+ production.

captures result in a visible energy above 5 MeV. Moreover, for neutrons which enter the tank, the n must traverse 6.7 interaction lengths (40 cm) of Gd-doped scintillator in order to reach the fiducial volume. The resulting rejection is about 0.001. We therefore take this background to be negligible in this study.

5.4 Stopping-muon-induced ^{12}B

Cosmic ray muons entering the detector may capture and produce ^{12}B which β decays. Capture occurs 8% of the time in oil [33]. Because only the μ^- captures, we gain a factor of two. The rate of stopping muons which capture is therefore $0.042\text{Hz} \times 0.04 = 0.002$ Hz. Only 19% of these events, however, appear in the $3 < E_{vis} < 5$ window. The rate is therefore on the order of 0.0003 Hz. This represents more than 24,000 events per detector during the run, which is far too high a level of background for this analysis. To reduce the rate further, we introduce the stopping muon veto, which is described in section 2.3.1. The 200 ms veto window represents about ten lifetimes. We therefore expect no ^{12}B background events in the two near detectors.

5.5 High-energy-muon-induced Isotopes

High energy cosmic rays produce β decaying isotopes in a number of ways. Spallation refers specifically to nuclear disintegration due to interaction with a virtual photon, although the term is often used loosely. Other sources are elastic and inelastic scattering. High energy secondary neutrons and pions can also produce isotopes, so that modeling the transport and interaction

Isotope	E_{vis} Cut (MeV)	decay-correlated n	muon-neutron veto	Final rate
^{9}Li	0.18±0.03 (19%)	0.09±0.02 (50%)	N/A	0.09±0.02
^{8}He	0.29±0.08 (30%)	0.24±0.07 (84%)	N/A	0.24±0.07
^{8}Li	0.47±0.19 (13%)	N/A	0.15±0.06 (32%)	0.15± 0.06
^{6}He	0.29±0.05 (2%)	N/A	N/A	0.29±0.05
^{9}C	0.53±0.17 (12%)	N/A	0.02±0.01 (3%)	0.02±0.01
^{8}B	0.65±0.16 (10%)	N/A	0.02±0.01(3%)	0.02±0.01

Table 6: Isotopes decays/detector/day after each cut, applied sequentially. Error is on the cross section measurement from reference [10]. Value in parenthesis is the percent of the original rate retained after the cut.

.

of secondaries is important. As will be mentioned below, calculations using measured isotope production rates by muons are in fairly good agreement with the observations at KamLAND and can thus be used to estimate the background rates for this measurement. The sources for muon-induced β-decaying isotopes of particular concern for this analysis are listed in Table 1.

5.5.1 Predicted Rates

The raw rates for a 13 ton fiducial volume scintillator-oil-based detector located under a 300 mwe overburden are shown in column 5 of Table 5. These rates were based on results from the NA54 experiment at CERN which studied isotope production from ^{12}C using 100 and 190 GeV muon beams[10]. The error on the reported rates comes from the error on the cross section measurement[10], and represents a potential systematic in the result if the rates cannot be understood in other ways.

The signal from ^{9}Li and ^{8}He were indistinguishable in the NA54 data, and hence are grouped together here. The KamLAND experiment is studying the relative rates of these two decays, and may be able to make measurements of the individual cross sections in the near future. For the sake of argument here, we assume that the contributions of ^{9}Li and ^{8}He are equal for the measured rate in NA54, although we consider this further below. It should be noted that if the relative rates of the two processes are not determined, then one needs to include a systematic which covers the range from the assumption of 100% Li to 100% He.

By taking the fraction of events in a 3 to 5 MeV window, assuming the correct β-decay spectrum, we obtain the approximate rate with the energy cut, shown in Table 6, column 2. At the time of the β decay, a neutron accompanies 50% of the ^{9}Li decays and 16% of the ^{8}He decays and these events will not contribute to elastic scattering background. One therefore obtains the rates shown in column 3.

In column 4, we show the result of introducing the muon-neutron veto. This addresses the cases where the muon interaction produces neutrons as well as a beta-decaying isotope. Neutrons will be liberated when ^{8}Li, ^{9}C, and ^{8}B are produced from a muon interaction with ^{12}C. A two component veto, requiring a muon signal and a neutron signal, can therefore reduce the background from these isotopes. This is described in Section 2.3. The neutron component of the veto must aim to identify up to three neutron captures during a time-window following the muon, as is consistent with the production of ^{9}C, and ^{8}B. This veto is expected to be applied at the analysis level.

The final rate is given in column 5. The total is 0.81±0.11(sys) events/day per detector or 1458±198 for both detectors. This leads to a systematic error of nearly 2% in the 10000 event signal, which is at least a factor of two higher than can be accepted if the goal is to match the NuTeV errors. Note that if the relative rates of ^{9}Li+^{8}He are not untangled, that the final rate for the combination becomes 0.33±0.15. This leads to a total of 0.81±0.17(sys) events/day per detector, or an even larger systematic error from these event. Furthermore, with a process as involved as spallation production of isotopes, it is crucial to constrain this systematic from the data. It is therefore clear that we must find a better method for addressing this issue.

5.5.2 Use of the Far Detectors to Reduce the Systematic Error

The far detectors are an ideal place to cross check the predictions for muon-induced isotopes, because the signal is less than 5% of the background at the far detector. When one applies all of the analysis cuts, one isolates the contribution from environmental backgrounds to the signal region. These backgrounds mainly come from high energy muon-induced isotopes, but there is also a contribution of about 100 events from contaminants (see section 5.1.3). One does not expect the environmental backgrounds to be a flat distribution in the visible energy window, as can be seen in Fig. 4

The far detector measurements can constrain the near detector back-

grounds only to the extent that all detectors are built identically. The design feature which is likely to be least similar between the near and far detectors is the overburden. Despite the homogeneity of the rock in the Braidwood area, the overburden for the near and far detectors may well differ by $\sim \pm 10$ mwe for shafts of identical depth.

With overburden differences of $\sim 3\%$, the rate of high energy muon production of isotopes will differ in the near and far detectors. However, for such small variations in overburden, one expects shifts in the normalization, but no significant deviation as a function of energy. We propose two methods for correcting the background normalization between the near and far detectors.

The first method is to correct the normalization in the far detector using the ratio of cosmic ray rates in the near compared to the far detectors. Given a cosmic ray rate of 3.5 Hz per detector, one expects more than 3×10^8 cosmic ray events per year in each detector. The statistical error in the normalization correction is therefore negligible. We will assume that this is the method which is employed, and not consider an error from the normalization correction.

The second method uses the high energy ($E > 10$ MeV) β-decays to normalize the near-to-far detector rates. This cut is chosen to be sufficiently high so that in the near detector, inverse beta decay, and elastic scattering events do not contaminate the sample. It is sufficiently low, however, that we expect about 4500 events per detector, allowing a high statistics measurement. It should be noted that this sample is not contaminated by Michel electrons or ^{12}B, due to the stopping muon veto. Given two near detectors we expect 9000 events. The correction for the ^{12}B decays which escape the stopped muon veto is well understood based on the large sample of identified decays. The error on the normalization from this method is consequently about 1%. This is sufficiently small to serve as a useful cross check for the correction based on relative cosmic ray rates. Note that all of the isotopes except for ^{6}He and ^{8}He contribute to $E > 10$; this is therefore a direct check of the dominant sources of isotopes.

The reactor-induced events in the far detector must be subtracted. At 1.8 km from the reactor core, the signal rate and the $\bar{\nu}p$ backgrounds are both reduced by the factor $(0.2/1.8)^2 = 0.01$. One therefore expects only about 50 signal events and 13 inverse beta decay background per detector, compared to over 650 events from the environmental backgrounds.

Assuming that we combine the information from all four far detectors, we will have $2920 \pm 54(stat) \pm 16(signal\ subtraction)$. The errors from statistics

	25 mwe	50 mwe	300 mwe	450 mwe
muons (m^{-2} s^{-1})	88.3	24.6	0.53	0.19
neutrons (ton^{-1} day^{-1})	11360	4942	322	145
^{9}Li+^{8}He	5.3±0.9	2.3±0.3	0.15±0.02	(6.6±0.7) × 10^{-2}
^{8}Li	10.±5.	4.4±1.9	0.28±0.11	0.13±0.05
^{6}He	40.±12.	17.±4.5	1.1±0.2	0.50±0.07
^{9}C	12.1±5.3	5.2±2.1	0.34±0.11	0.15±0.05
^{8}B	17.9±6.4	7.7±2.5	0.50±0.12	0.22±0.05

Table 7: Isotopes with energy endpoint > 3 MeV for various overburdens. Rate for the isotopes is in decays/ton/d.

and signal subtraction can be combined in quadrature to yield ±56 events total. This measurement will therefore lead to an error of approximately 0.5% on the signal. We can combine this with the first principles calculation of section 5.5, because this is an independent method for determining the background. Combining the two approaches yields 1458±38(stat)±53(sys) events.

5.5.3 Comment on Overburden

Our canonical overburden is 300 mwe equivalent. At the Braidwood site, however, it is possible to reach 450 mwe. Larger overburden is advantageous to this analysis. The core-to-detector distance increases by $\sim 10\%$, but the rate of isotope production in the 3 to 5 MeV range drops by more than a factor of two, as shown in Table 7 (top). As a result, we recommend that 300 mwe be regarded as a minimum and that the detectors be constructed with the maximum feasible overburden.

If this experiment is performed at a facility where the overburden between near and far detectors varies substantially, so the far detector cannot be used to constrain the near detector, then an overburden which is deeper than 300 mwe is recommended. One can use the $E > 10$ MeV rates in the near detector to somewhat constrain the errors, but this does not significantly reduce the number of background events below 198. An overburden of 450 mwe will achieve approximately 100 events background, which is not ideal but still tolerable.

On the other hand, a shallow overburden cannot be tolerated due to

the high cosmic ray rate as shown in Table 7. For example, for 50 mwe, the through going cosmic ray rate increases by almost a factor of 15. The stopping rate will be substantially larger. This will lead to intolerable backgrounds from ^{12}B and high-energy-muon-induced isotopes.

5.6 Summary of Environmental Backgrounds

In summary, the environmental backgrounds come from two sources. The first source is decays of U and Th, which contribute about 100 events. Isotopes induced by high energy muons represent a much more serious background. For the calculation of $\sin^2\theta_W$, we will assume a total (U/Th and muon-induced isotopes) of 1558$\pm$39(stat)$\pm$53(sys) events.

6 The $\bar{\nu}p$ Normalization Sample

The $\sin^2\theta_W$ measurement requires that the absolute $\overline{\nu}_e$ flux be known with good accuracy. The flux can be measured in a straightforward manner using the high statistics sample of $\overline{\nu}p$ inverse beta-decay events. This process is illustrated in Fig. 7. There is a one-to-one correspondence between visible energy and neutrino energy for these events:

$$E_\nu = E_{vis} + 1.8 - 2m_e \ .$$

As shown in Fig. 7(top), therefore, the events can be binned as a function of E_ν. The $\overline{\nu}p$ inverse beta-decay cross section, shown in Fig. 7 (middle), is very well known, both in shape and magnitude, from measurements of the neutron lifetime. This has an uncertainty of 0.2%. As a result, the flux can be extracted for neutrinos above the threshold energy for inverse beta decay, see Fig. 7 (bottom). This is the same flux which contributes to our signal events.

In order to extract the predicted number of signal events, we use the procedure illustrated by Fig. 8. The top plot in this figure shows the cross section for elastic scattering events with 3 to 5 MeV visible energy as a function of E_ν. Multiplying this cross section by the flux in Fig. 7 (bottom), results in a total number of elastic scattering events with the visible energy cut, binned as a function of E_ν. This distribution is shown in Fig. 8 (middle). To see this, we rebin these events according to E_{vis} and we obtain Fig. 8

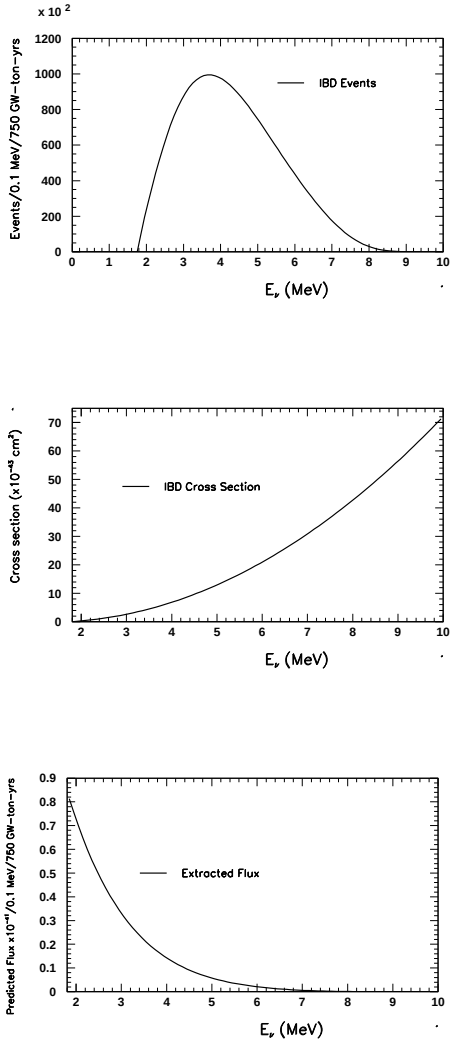

Figure 7: Illustration of method for extracting the flux. Top: inverse beta decay events *vs.* neutrino energy. Middle: predicted cross section for inverse beta decay events. Bottom: Extracted flux obtained from dividing the event distribution by the predicted cross section.

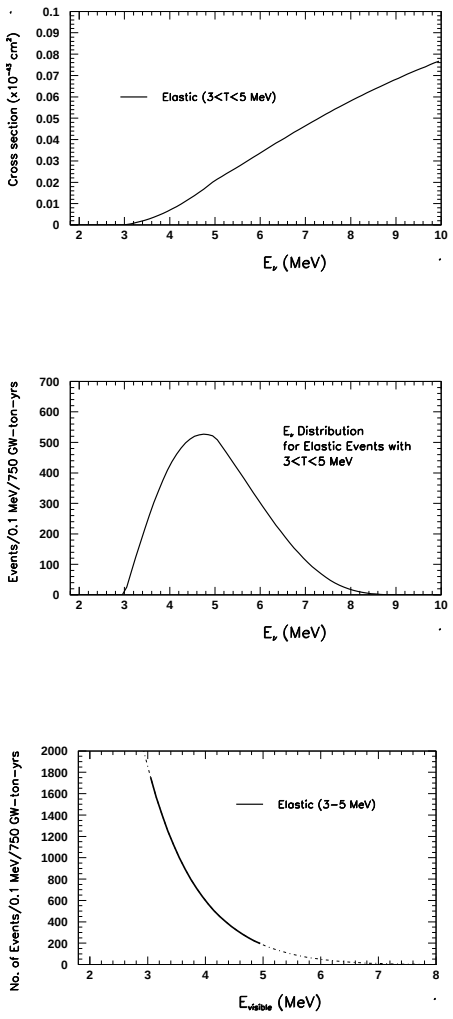

Figure 8: Illustration of method for comparing elastic scattering interaction prediction to data. Top: elastic scattering cross section, for interactions with visible energy between 3 and 5 MeV, for arbitrary $\sin^2\theta_w$, shown as a function of neutrino energy. Middle: resulting predicted event rate when the cross section (top) is multiplied by the flux distribution (Fig. 7, bottom). Bottom, bold: Rebinning of predicted event rate as a function of E_{vis}. Dotted line shows how the prediction would extend beyond the energy window. This predicted distribution will be compared with data.

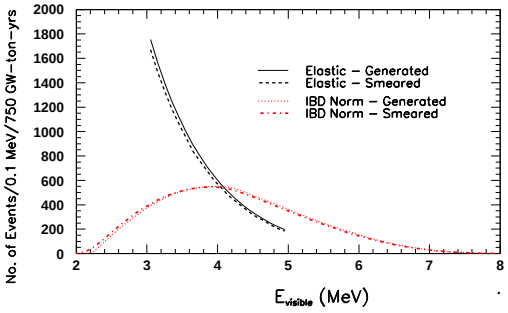

Figure 9: Comparison of generated and smeared visible energy distributions. Solid, Black: elastic scattering, generated; Dashed, Black: elastic,scattering smeared; Dotted, Red: inverse beta-decay generated; Dot-dashed, Red: inverse beta-decay smeared. The inverse beta-decay events (IBD Norm) have been weighted by the elastic to inverse beta-decay cross section ratio.

(bottom). This distribution is the prediction which we will then compare with data.

We will then vary $\sin^2\theta_W$ in the cross section, Fig. 8 (top), to obtain the best agreement between data and prediction. While the sensitivity is expected to mainly rely on normalization, the shape comparison will provide an important cross check.

The error in the $\overline{\nu}e$ event prediction as a function of $\sin^2\theta_W$ has contributions from statistical and systematic uncertainties. The statistical uncertainty is related to the $\overline{\nu}p$ inverse beta-decay event sample used to determine the flux. For the assumed "generic experiment" described here, there are about 2.7×10^6 $\overline{\nu}p$ inverse beta-decay events which, when weighted by the cross section ratio of $\overline{\nu}_e e$ to $\overline{\nu}p$ interactions and Gd capture fraction, yields an effective number of 1.58×10^6 events. As a result, the statistical error associated with the flux normalization and energy dependence is very small due to the high statistics, giving a contribution of $1/\sqrt{1.6 \times 10^6}$ or 0.08%.

The elastic scattering events have a substantially different visible energy distribution, as compared to the inverse beta-decay events after weighting for the elastic to inverse beta-decay cross section ratio; this can be seen in

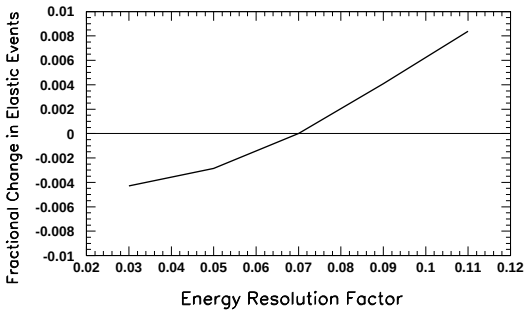

Figure 10: Change in number of elastic scattering events versus energy resolution factor.

Fig. 9. The reconstructed energy resolution smearing will therefore affect the two distributions differently, and a correction will need to be applied when using the inverse beta decay events for the elastic event prediction. Assuming an energy resolution of $\Delta E/E = 0.07/\sqrt{E(MeV)}$, the number of elastic scattering events in the $3 < E_{Visible} < 5$ MeV region goes down by 5%, but the sum over the full region of the weighted inverse beta decay events changes very little, as seen in Fig. 9. One therefore needs to make a correction using a Monte Carlo simulation of the smearing and apply it to the prediction. This correction will depend on knowing the energy resolution for the detector. Fig. 10 shows the fractional change in the predicted number of elastic scattering events versus the energy resolution factor k used in the parameterization, $\Delta E/E = k/\sqrt{E(MeV)}$. Sources and other types of calibrations will be used to determine k for the experiment. For now, it is assumed that $k = 0.07$ with an uncertainty of 10% or ± 0.007. As seen from Fig. 10, this gives a systematic error on the normalization of 0.1% due to the uncertainty in k. This is negligible for the analysis.

An important systematic error associated with the normalization is the number of free protons in the oil, which is correlated to the number of electrons available as targets for elastic scattering. In fact, the fractional error on the number of electrons is 75% of the error on the number of free protons. CHOOZ determined the number of free protons by burning the oil [6],

yielding a measurement accurate to 0.8%. Assuming we can do no better, the fractional error on the number of electrons is, therefore, 0.6%.

Another important systematic is the error on the fraction of neutrons which will be tagged by a Gd capture. As discussed in section 1, we use this sample because it selects events with negligible background. For a systematic error estimate, we assume that $84 \pm 0.25\%$ events will capture on Gd.

7 Calculating the Error on $\sin^2\theta_W$

We first obtain the error on the number of signal events and then extract the error on $\sin^2\theta_W$. The terms which contribute to the error on the number of signal events are: 1) the statistical error on the signal; 2) the statistical and systematic errors associated with the $\bar{\nu}p$ background; 3) the statistical and systematic errors associated with the environmental backgrounds; and 4) the statistical and systematic errors associated with the normalization.

For the first calculation, we assume the standard set of proposed cuts. Next, we consider what is required to reach the NuTeV level of error. Then, we consider the impact if the experiment has less scintillator purity than proposed here. Lastly, we consider the impact if there is substantially more background from isotope decays than expected.

7.1 Error on $\sin^2\theta_W$ for the Proposed Analysis

In this section, we consider the contribution of each error source. A summary of each of the sources, along with the fractional error on the number of $\bar{\nu}e$ events, is shown in Table 8. Where the contribution to the error was negligible (< 10 events), we list 0% error.

The statistical error on the signal is calculated using the number of elastic scattering events within the $3 < E_{vis} < 5$ MeV window, N_e. We find that for 900 days live-time, $N_e = 11,440$ events.

The statistical error from the $\bar{\nu}p$ background subtraction is $\sqrt{N_{p\ bkgd}}/N_e$. $N_{p\ bkgd}$ is given by the number of $\bar{\nu}p$ events passing the signal cuts, N_p, multiplied by the inefficiency for identifying these events correctly, ϵ_p. For 900 days live-time, $N_p = 1,224,391$. In this analysis, $\epsilon_p = 0.12\%$, as discussed in section 4.4. $\sqrt{N_{p\ bkgd}}/N_e$ is the fractional error from the statistical error on this background. We assume that the systematic error on the $\bar{\nu}p$ background measurement is negligible (see section 4 for justification).

Statistical error on the signal	0.95%
Statistical error $\bar{\nu}p$ background subtraction	0.34%
Systematic error $\bar{\nu}p$ background subtraction	0.0%
Statistical error on U and Th background	0.09%
Systematic error on U and Th background	0.0%
Statistical error on muon-induced isotopes	0.34%
Systematic error on muon-induced isotopes	0.46%
Statistical error on the normalization	0.10%
Systematic error on electron-to-free-proton ratio	0.60%
Systematic error on the Gd capture fraction	0.30%
Total error	1.3%

Table 8: Fractional errors contributing to the error on the number of $\bar{\nu}e$ scattering events based on assumptions presented in this paper. Negligible sources of error are taken to be 0% here (see text). To equal the NuTeV error, 1.2% total error was required.

The environmental backgrounds contribute both statistical and systematic errors. Let $N_{env\ stat}$ be the contribution from the statistical error. Similarly, $N_{env\ sys}/N_e$ is the contribution from the systematic error on the environmental backgrounds, $N_{env\ sys}$. We list the contribution from U and Th and muon-induced isotopes separately in table 8. The systematic error on the contaminants is negligible but the systematic error on the isotopes, ± 53 events, must be considered.

The statistical error on the normalization sample is extracted using $N_{n\ eq}$, the number of equivalent $\bar{\nu}p$ events weighted by the cross section ratio (see section 6). We find that $N_{n\ eq} = 1,582,900$. For the setup we describe, this includes an adjustment by 84%, since the normalization sample uses only events which capture on Gd. The first systematic error on the normalization sample comes from knowledge of the number of electrons in the sample. As discussed in section 6, this is tied to the knowledge of the number of free protons and is $dN_{free\ p}/N = 0.6\%$. The second significant systematic error on the normalization sample comes from the error on the knowledge of the Gd capture fraction. We have argued that 0.25% can be attained.

Adding the systematic errors in quadrature, we find $(dN/N)_{sys} = 1.0\%$. Adding this in quadrature with the statistical error on the signal yields $(dN/N)_{tot} = 1.3\%$. This is close to the goal of 1.2% which we set at the

start of this paper. Extracting the error on $\sin^2\theta_W$, we obtain: $\delta(\sin^2\theta_W) = 0.0019$. This is comparable to the NuTeV error of 0.0017.

7.2 Improving this Measurement

As one can see from Table 8, the error on $\sin^2\theta_W$ is dominated by statistics. If the running period were doubled to 1800 days, one would achieve $\delta(\sin^2\theta_W) = 0.0016$. Alternatives to increased running period include enlarging the detector, adding extra near detectors, finding a closer approach to the reactor cores, or moving to a more powerful reactor. Any of these options will substantially improve the result.

The rate of production of muon-induced isotopes can be reduced by using a larger overburden. If the rate reduced by a factor of two by going to 450 mwe, then the error on $\sin^2\theta_W$ drops by 0.00003. If we have a 450 mwe overburden and the experiment runs for 1800 days, the experiment attains $\delta(\sin^2\theta_W) = 0.0015$. Reduction of these background events may also be achieved by a better muon-neutron veto. If the veto introduces excessive deadtime, however, then the loss in elastic scattering statistics may offset the gains in background reduction.

7.3 Impact of Impurities of the Gd-Dopant

We have assumed that KamLAND levels of purity for U and Th (5×10^{-17} g/g Th) can be achieved. The techniques for purifying oil have been established by CTF and KamLAND and therefore appear to be practical. This experiment, however, requires that Gd dopant be added to the oil. Experience from CHOOZ [6] indicates that this can introduce a high level of Th contamination, so purification of the Gd will need to be researched.

To establish the effect of increased contamination, consider the change in the error as the contamination is increased. In our calculation above, with 100 Th and U induced events in the E_{vis} window, we achieved $\delta(\sin^2\theta_W) = 0.0019$. One order of magnitude increase in contamination results in $\delta(\sin^2\theta_W) = 0.0020$. Two orders of magnitude increase in U and Th contamination gives $\delta(\sin^2\theta_W) = 0.0023$. These are both within a tolerable range, especially given that running longer will still have a substantial effect on reducing the error. Three orders of magnitude larger contamination, however, renders the result uninteresting, with $\delta(\sin^2\theta_W) = 0.0046$. This constrains

the necessary level of purity which must be achieved to better than 5×10^{-15} g/g of Th.

7.4 Impact of Increased Isotope Background

We have calculated the background from β-decaying isotopes based on calculations from reference [10]. We did not, however, include the background from ^{11}Be, for which only a gross upper limit has been set [10]. Using this upper limit as an expected level of isotope production increases the background from 1458 to 1803 events. This produces a negligible shift in $\delta(\sin^2\theta_W)$. In fact, increasing the total isotope background by a factor of two only increases $\delta(\sin^2\theta_W)$ to 0.0020.

8 Conclusions

This paper discusses a technique for measuring $\sin^2\theta_W$ at a reactor-based experiment using $\bar{\nu}e$ elastic scatters. A precise measurement of $\sin^2\theta_W$ at $Q^2 \approx 4$ MeV^2 and using neutrinos as probes opens a window for tests of neutrino properties and the electroweak theory. We have used an experimental design which is consistent with many proposals for near detectors at reactor-based oscillation experiments. We have also assumed realistic reactor power and a human-scale run time of about 900 days.

The analysis has statistical and systematic errors which are roughly equal, so increased statistics will yield further improvement. At least ∼26 tons of fiducial volume are required and the detector should be located as close as possible to the reactor (∼ 250 m or less).

We have also introduced the idea of normalizing to the $\bar{\nu}p$ events. This substantially reduces the error from the flux. Because the normalization sample is measured in the same detector as the elastic scattering signal, many systematics effectively cancel, including those associated with deadtime and fiducial volume.

We have also considered backgrounds from misidentified inverse beta decay events. Using n-identification and a visible energy window, this background can be reduced to an acceptable level. Environmental background is dominated by the contribution from spallation by cosmic ray muons which produce isotopes which β-decay. To attain acceptable rates, 300 mwe overburden is the minimum required. Indeed, deeper overburden is desirable.

Future studies on reducing this background by identifying muons which spallate are important. It is also necessary to maintain oil and Gd purity from U and Th contaminants. Our calculations show that KamLAND-levels of purity are desirable, but an increase of two orders of magnitude of impurity is acceptable.

This exercise was meant to serve as a proof-of-principle that a reasonable error on $\sin^2\theta_W$ can be attained at a reactor-based experiment. The technique has not yet been fully optimized. The total error which we obtain on $\sin^2\theta_W$ is $\delta(\sin^2\theta_W)$=0.0019. This is comparable to the NuTeV error of 0.0017. This error is lower than the published SLAC E158 and APV results. A measurement at this precision will uniquely probe the electroweak and neutrino sectors. Therefore, we conclude that the idea is feasible and more detailed studies are warranted.

Acknowledgments

We thank G. P. Zeller and the Columbia Neutrino Group for their input. Also, we thank T. Bolton, J. Formaggio, K. Heegar, G. Gratta, W. Louis, D. Naples, P. Nienaber and P. Vogel for their comments.

References

[1] G. P. Zeller *et al.*, Phys. Rev. Lett., **88** 091802, 2002.

[2] S. C. Bennett and Carl E. Wieman, Phys. Rev. Lett., **82** 2484–2487, 1999.

[3] M. Woods [SLAC E158 Collaboration], hep-ex/0403010, 2004; P. I. Anthony, et al., hep-ex/0312035, submitted to PRL, 2003.

[4] R. Carr *et al.*, SLAC-PROPOSAL-E-158, 1997.

[5] F. Reines, H. S. Gurr, and H. W. Sobel Phys. Rev. Lett., **37** 315–318, 1976.

[6] M. Apollonio *et al.*, Eur. Phys. J., **C27** 331–374, 2003.

[7] K. Anderson *et al.*, hep-ex/0402041, 2004.

[8] Z. Daraktchieva *et al.*, Phys. Lett., **B564** 190–198, 2003.

[9] Karsten Heager, private communication.

[10] T. Hagner *et al.* Astropart. Phys., **14** 33–47, 2000.

[11] Carlo Bemporad, Giorgio Gratta, and Petr Vogel, Rev. Mod. Phys., **74** 297, 2002.

[12] O. Ju. Smirnov, INFN/TC-00/17. 2000.

[13] K. Eguchi *et al.* Phys. Rev. Lett., **90** 021802, 2003.

[14] A. Baldini *et al.* Nucl. Instrum. Meth., **A389** 141–145, 1997.

[15] L. Bugel *et al.*, FERMILAB-PROPOSAL-937. hep-ex/0402007, 2004.

[16] G. Alimonti *et al.*, Astropart. Phys., **16** 205–234, 2002.

[17] J. M. Link, In *Intersections of Particle and Nuclear Physics*, **AIP** 698, 771-774, 2003.

[18] A. A. Aguilar-Arevalo *et al.*, The MiniBooNE Run Plan, available at http://www-boone.fnal.gov/publicpages/news.html, 2003.

[19] G. Alimonti *et al.*, Astropart. Phys., **8** 141–157, 1998.

[20] Donald E. Groom, Nikolai V. Mokhov, and Sergei I. Striganov, Atom. Data Nucl. Data Tabl., **78** 183–356, 2001.

[21] F. M. Newcomer and R. Van Berg, IEEE Trans. Nucl. Sci., **42** 745–749, 1995.

[22] M. R. Adams *et al.*, Phys. Rev. Lett., **74** 5198–5201, 1995.

[23] K. Hagiwara *et al.*, Phys. Rev., **D66** 010001, 2002.

[24] Y. F. Wang *et al.*, Phys. Rev., **D64** 013012, 2001.

[25] D. I. Garber and R. R. Kinsey, BNL325, 1976.

[26] M. Fukugita and S. Yazaki, Phys. Rev., **D36** 3817, 1987.

[27] J. M. Lattimer and J. Cooperstein, Phys. Rev. Lett., **61** 23–26, 1988.

[28] Riccardo Barbieri and Rabindra N. Mohapatra, Phys. Rev. Lett., **61** 27, 1988.

[29] G. G. Raffelt, Phys. Rept., **320** 319–327, 1999.

[30] D.H. Wilkenson, Nucl. Phys., **A337** 474, 1982.

[31] Donna Naples, private communication.

[32] G. L. Cassiday, J. W. Keuffel, and J. A. Thompson, Phys. Rev., **D7** 2022–2031, 1973.

[33] T. Suzuki, David F. Measday, and J. P. Roalsvig, Phys. Rev., **C35** 2212, 1987.

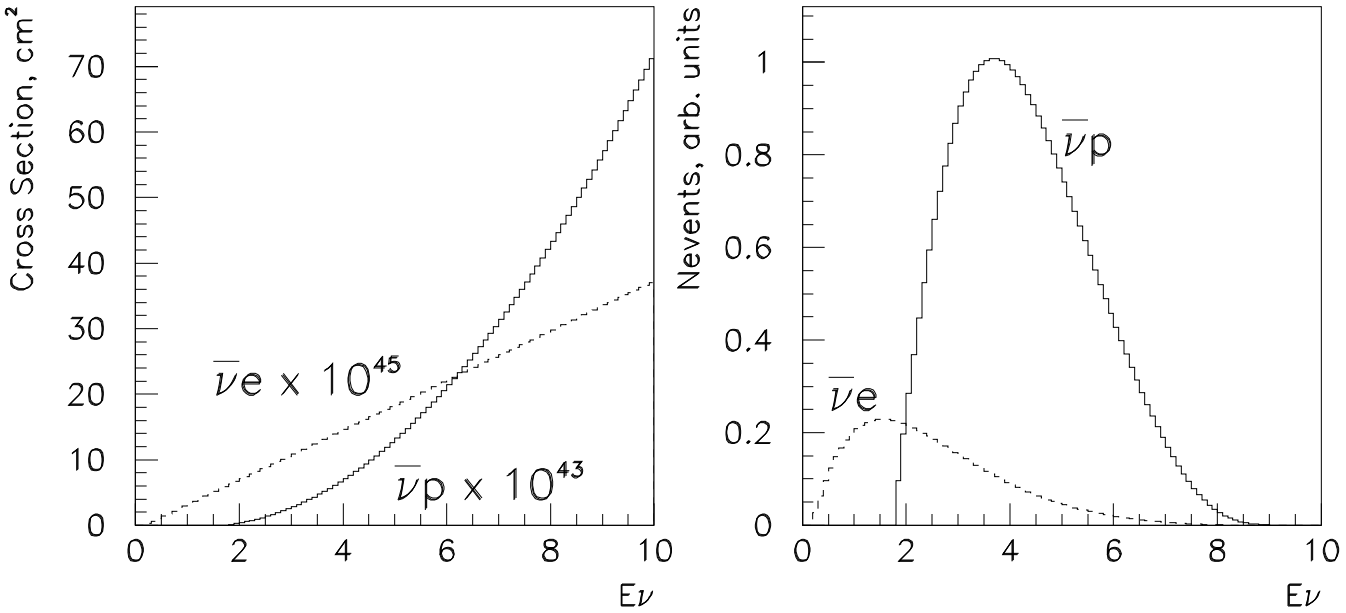
Cross Section, cm²
70
60
50
40
30
20
10
0
0
2
4
6
8
10
Eν
$\bar{\nu}$e x 10⁴⁵
$\bar{\nu}$p x 10⁴³
Nevents, arb. units
1
0.8
0.6
0.4
0.2
0
0
2
4
6
8
10
Eν
$\bar{\nu}$p
$\bar{\nu}$e